TSX INSAR ASSESSMENT FOR SLOPE INSTABILITIES MONITORING IN ALPINE PERIGLACIAL ENVIRONMENT (WESTERN SWISS ALPS, SWITZERLAND)

Chloé Barboux[(1)], Reynald Delaloye[(1)], Tazio Strozzi[(2)], Claude Collet[(1)], Hugo Raetzo[(3)]

[(1)] Dept. of Geosciences, Geography, Univ. of Fribourg, 1700 Fribourg, Switzerland, [name.surname]@unifr.ch
[(2)] Gamma Remote Sensing, Worbstr. 225, 3073 Gümligen, Switzerland, strozzi@gamma-rs.ch
[(3)] Federal Office for the Environment, 3003 Bern, Switzerland, hugo.raetzo@bafu.admin.ch

ABSTRACT

The potential of Terrasar-X (TSX) InSAR for the acquisition of high resolution X-band interferograms with an 11 day time interval has been investigated for the monitoring of creeping landforms in the alpine periglacial belt. In order to give a reliable assessment of InSAR visibility, an index characterizing the velocity compression is calculated for 30 surveyed landforms like rockglaciers, landslides and debris covered glaciers. Results show that the monitoring of some very active rockglaciers (1-3.5m/y) may be possible when the latter are not hidden by layover or shadow. Moreover, compared to lower resolution data, TSX is well suitable to monitor active landforms. Even if field measurements are, in most cases, still needed to validate and confirm observations at local scale, TSX InSAR appears to be an efficient remote sensing method to monitor slope instabilities in this environment.

1. INTRODUCTION

The Western Swiss Alps, here also called Valais, cover a large surface of more than 5000 km^2. It extends east of Mont-Blanc from the Bernese Oberland to the north, through the Rhone Valley and the Penninic Alps (Entremont, Bagnes, Hérens, Anniviers, Turtmantal, Mattertal, Saastal with the famous peaks Grand Combin, Dent Blanche, Dom, Matterhorn, etc.), to the Swiss-Italian border to the south. Large parts of the area lie within the alpine or high alpine zone, which could be potentially influenced by permafrost. The lower limit of the discontinuous permafrost in the Valais Alps region is estimated at about 2400 m a.s.l. in north-facing slopes, and at about 2700 m a.s.l. in southern expositions [1,2], and potentially affects loose sediments (talus slopes, moraines, rock glaciers, landslides, etc.) as well as rock walls. Perennially frozen terrains are susceptible to move (permafrost creep) and their dynamics are partially controlled by the thermal state of permafrost. Any change in the permafrost creep rate (e.g. higher creep rates consecutive to a warming of permafrost) modifies the transfer rate of loose material along alpine slope and may affect the frequency, magnitude, as well as the type of related slope instabilities [3,4]. In the context of climate change and in view of natural hazard risk management in mountain areas, particularly in densely inhabited Alpine regions, there is a great need to investigate automated techniques to detect and monitor slope instabilities at both local and regional scales.

2. STUDIED AREA AND INSAR

Fundamental research on mass wasting dynamics in the Alpine periglacial belt (between 2300 and 3000 m a.s.l.) has been conducted in the Western Swiss Alps. The topography of this region, mainly consisting of north-south oriented valleys is optimal for an application of the InSAR technique. Since 2005, several inventories of InSAR detected slope instabilities (Fig. 1) have been compiled at a regional scale in this test region [5-9] using a large set of InSAR data archive (mainly ERS-1/2 and JERS data archive from 1991 to 2000). The alpine periglacial belt ï defined as the portion located above the lower limit of the discontinuous permafrost to the summits excluding glaciated areas ï covers about 50% of the Valais. More than 2000 landforms located in this belt, amounting to 4% of it, were detected with a velocity ranging from a few centimetres to several meters per year (Fig. 2).

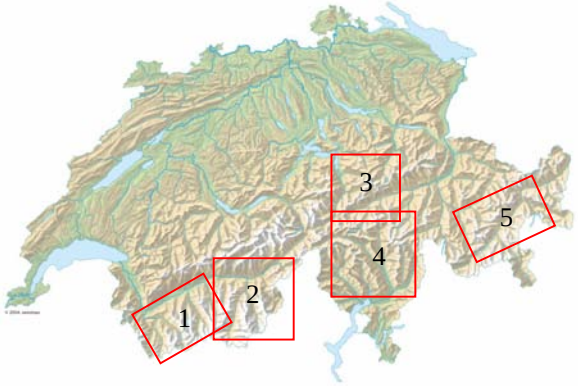

Figure 1: Project areas of systematic mass wasting inventories based on InSAR data in the Swiss Alps: lower Valais (1), Upper Valais (2), Gotthard-North (3), Ticino (4), Upper Engadine (5)

Proc. 'Fringe 2011 Workshop', Frascati, Italy,
19–23 September 2011 (ESA SP-697, January 2012)

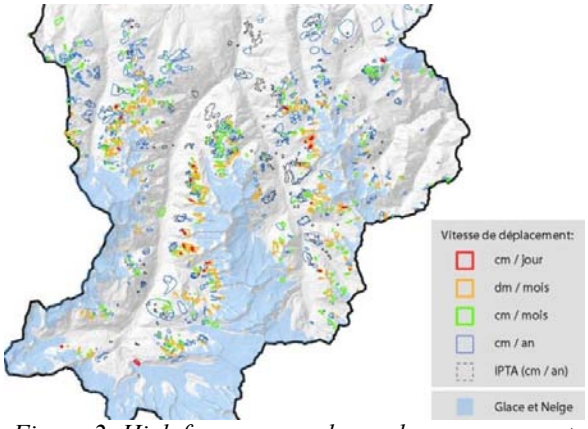

Figure 2: High frequency and complex arrangement of InSAR polygons above the tree line (Example from Upper Valais). Highest peaks culminate above 4000 m a.s.l. Glaciers in light blue.

Among all of these active landforms, 30 of them are annually or seasonally surveyed by GPS field measurements since 2000 for the longest series. The use of InSAR, especially ERS-1/2 InSAR, to estimate magnitude and spatial pattern of slope motion has been thus evaluated and verified on different selected sites with known phenomena and shows the efficiency of this remote sensing technology for inventorying creeping landforms in the mountain periglacial environment, but also for estimating and categorizing their displacement rates [10,11,12]. In particular, fast moving landforms were detected with ERS-1/2 1-day and 3-day repeated cycles data. InSAR has revealed to be the current best method for a large-scale survey of slope instabilities as it can be used to provide a regional overview of surface displacements at mm to cm accuracy over alpine areas, where dense vegetation and built-up areas are no longer present [12]. However, since the extinction of ERS-1/2 tandem, the higher deformation rate of rapidly moving rockglaciers (>1 m/y) can no longer be detected or surveyed correctly on C-band and L-band monthly SAR interferograms [3,4]. Thus, the goal of this study is to investigate the potential of TSX high resolution X-band interferograms with 11 days time interval for monitoring very active landforms, and to know how to use these data for further investigations.

3. TERRASAR-X INSAR VISIBILITY ASSESSMENT

In order to provide a reliable assessment of InSAR visibility for slope motion monitoring, a map of visibility characterizing the velocity compression is calculated. The index value ranging between 0 and 1 is used to determine the suitability of TSX to monitor each of our 30 surveyed test-landforms.

3.1. Visibility Mask Calculation

The first step consists of excluding areas polluted by irreversible geometric distortions. This mask is used to exclude invisible areas (shadows) and also reverse imaged areas (layover). Layover and shadow evaluation is already well explained and computed in literature [13, 14]. As this mask does not differ between acquisitions of scenes using both the same mode and incidence angle, it does not need to be computed for each InSAR pair. Finally, the result only gives a binary characterization of the InSAR visibility (1 = yes; 0 = no).

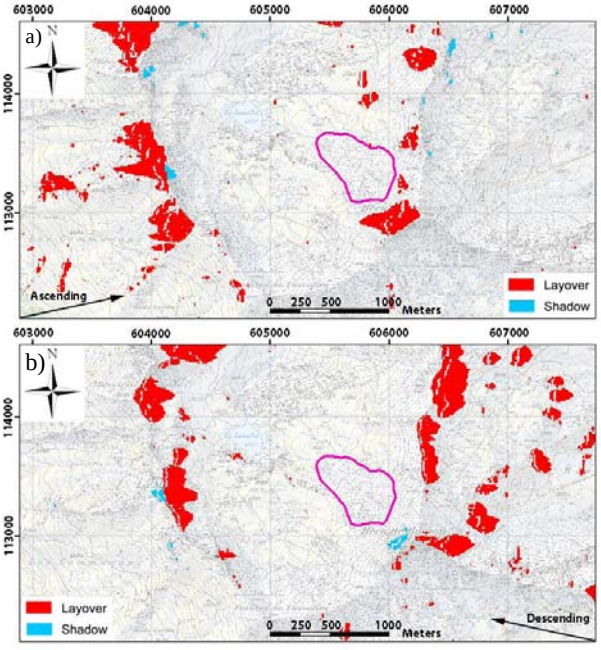

Figure 3 : Examples of layover and shadowing masks in a) ascending and b) descending mode (Vallon de Réchy).The pink polygon is the active Becs-de-Bosson rockglacier, monitored by terrestrial surveying since 2001.

3.2. Visibility Map Calculation

The second step consists of determining a quality index, ranging between 0 and 1, which characterizes the InSAR visibility. The quality of the observation is evaluated here for the displacement on a unit area of the ground surface which is directly related to the topography and the look angle.

Assuming the flow direction to be down slope everywhere, the three components of the displacement in the highest slope direction v_{HS} could be estimated. In order to give a reliable assessment of InSAR visibility for slope motion monitoring, an index of visibility *RdHS* characterizing the velocity compression for each landform cell is computed. Under the hypothesis that the landform flow is directed toward the highest slope angle direction at 25m scale resolution, *RdHS* is defined

as the dot product between the unit vector in the maximum slope direction and the unit vector in the line of sight (LOS) direction.

Let:
- v_{LOS} the displacement projected in the LOS direction.
- e_{LOS} the unit vector of the displacement in the line of sight direction
- e_{HS} the unit vector of the flow in the highest slope direction

Then, from $v_{hs} = \frac{v_{LOS}}{e_{LOS} \cdot e_{HS}}$ (1)

The projection coefficient Rd_{HS} is defined by the dot product of e_{LOS} and e_{HS}:

$$Rd_{HS} = e_{LOS} \cdot e_{HS}$$
$$= e_{LOS|x} \cdot e_{HS|x} + e_{LOS|y} \cdot e_{HS|y} + e_{LOS|z} \cdot e_{HS|z} \quad (2)$$

With:

$$e_{LOS} = \begin{cases} \cos(Lv_\theta)\cos(Lv_\varphi) \\ \cos(Lv_\theta)\sin(Lv_\varphi) \\ \sin(Lv_\theta) \end{cases} \quad (3)$$

And

$$e_{HS} = \begin{cases} \cos(u)\cos(v - \pi/2 + Lv_\varphi) \\ \cos(u)\sin(v - \pi/2 + Lv_\varphi) \\ -\sin(u) \end{cases} \quad (4)$$

Rd_{HS} is the compression factor applied to the displacement in the direction of the highest slope for a considered image. As expected, there is no detectable variation of this map between acquisitions of a scene using same mode and incidence angle, thus it does not need to be computed for each InSAR pair.

In fig. 4, the displacement in the highest slope direction is reduced by 77% in ascending mode, while it is only reduced by 45% in descending mode. A substantial reduction could induce difficulties in interpreting velocities. However it could be very useful to monitor high velocity rates. Moreover, in ascending mode, the standard deviation of this indicator is 0.14, while it reaches 0.21 in descending mode, which means that even if the descending mode has a higher visibility index than the ascending one, the velocity of the landform will be less uniform in that case.

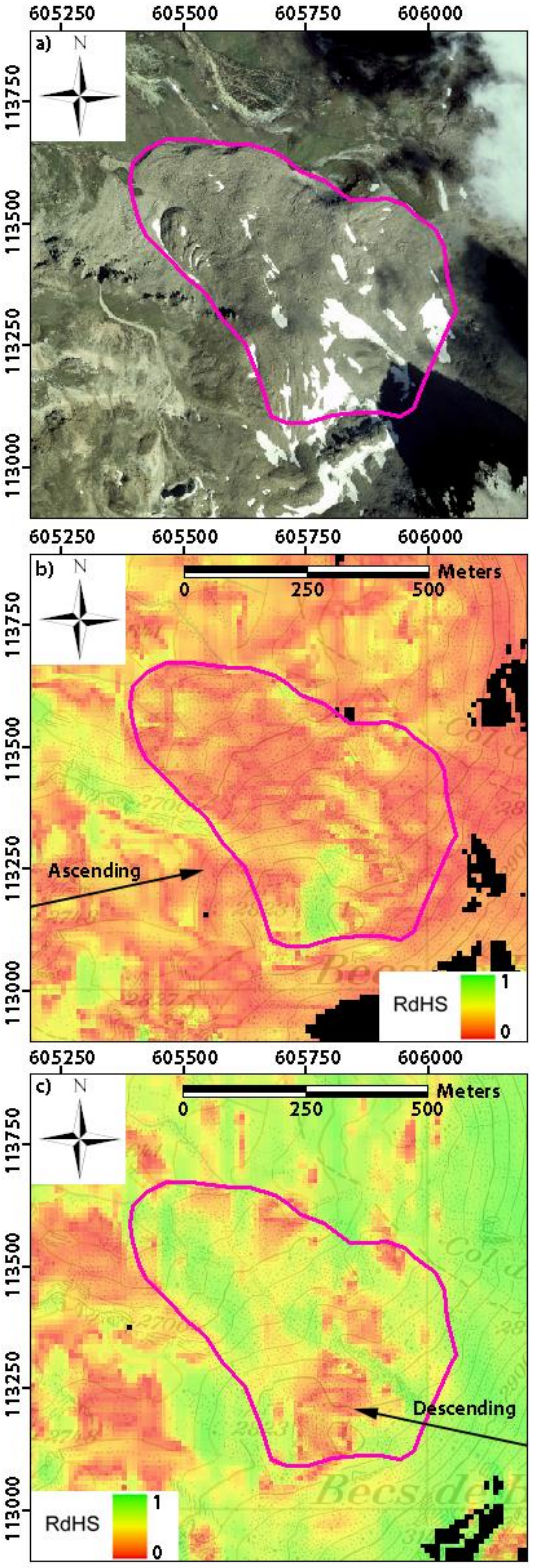

Figure 4: a) Orthoimage of the Becs-de-Bosson rockglacier, Vallon de Réchy (2005) and results of the visibility map compression in b) ascending and c) descending modes. RdHS goes from red (highly compressed) to green (no compression). Layover and shadow is masked in black

4. APPLICATIONS TO THE WESTERN SWISS ALPS

4.1. Testing sites

85.6% of the alpine periglacial belt in the Valais is visible by TSX InSAR. Remaining areas are either masked by layover or shadow, or not covered by our specific orbits. Almost 49.2% of this belt is visible in both modes. Our test sites consist of different landform types (18 rock glaciers, 1 push moraine, 9 landslides and 2 covered glaciers). Most of them are located on slope of about 25° and have an area smaller than 10ha. Their flows are more or less 11.6° directed toward the highest slope direction. Their distribution seems to be representative of the region by their locality, aspect, elevation as well as velocity (Fig. 5, 6 and 7). 97.1% of these landforms are visible by TSX either in ascending or descending mode in term of layover and shadow. Tab. 1 expresses the percent of visibility for each surveyed landform. When visibility does not exceed 50%, the analysis in the specified mode is turned down for the considered landform.

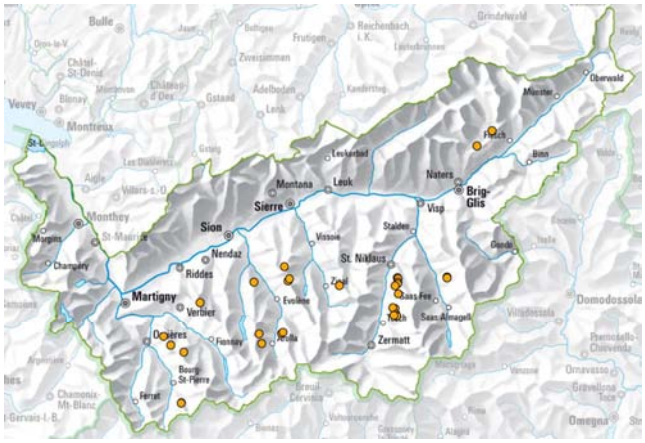

Figure 5 : Testing sites location in Valais

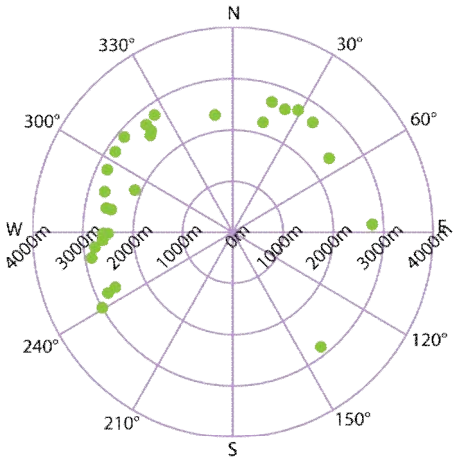

Figure 6 : Elevation and aspect of the 30 test sites

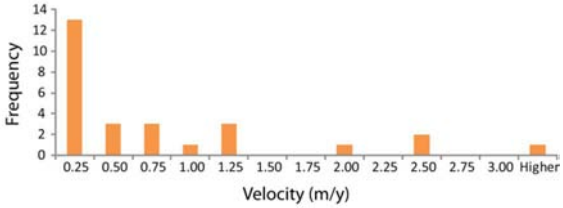

Figure 7 : Landforms annual velocity rate

ID	Name	Ascending %	Descending %
1	Petit Vélan	100	100
2	Petit Vélan (tot)	100	95.19
3	Aget	100	100
4	Mille	100	79.15
5	Six Blanc	90.46	100
6	Lapires	100	94.86
7	Vendes	100	100
8	Ignes	100	99.80
9	Mont Dolin	63.70	100
10	Perroc	38.76	100
11	Tsarmine	95.20	100
12	Réchy	99.96	100
13	Lona Rockglacier	100	98.86
14	Lona Push-moraine	100	99.60
15	Bonnard	46.70	99.89
16	Grosse Grabe Rockglacier	1.03	75.93
17	Grosse Grabe Landslide	1.04	97.57
18	Breithorn	49.85	96.44
19	Gugla	70.18	99.89
20	Laengenschnee	0.68	87.16
21	Dirru	94.78	100.00
22	Graben Gufer Landslide	34.52	72.26
23	Graben Gufer Rockglacier	63.71	99.08
24	Chessi RockGlacier	92.52	98.27
25	Chessi Glacier	78.28	97.69
26	Gänder	97.97	100
27	Jegi Rockglacier	91.73	99.02
28	Jegi Landslide	98.17	100.00
29	Moosfluh	x	98.95
30	Grosses Gufer	x	100

Table 1 : Visibility scores for the 30 landforms. Remaining areas are masked either by shadow or by layover

4.2. InSAR Visibility

The visibility map was computed for each of these landforms. Then the maximal deformation rate *Vmax* ï corresponding to the velocity gradient ï was computed. Actually, if the relative displacement between two neighboring pixels exceeds one fringe, it cannot be detected using InSAR [15]. Thus, the maximum detectable deformation rate is one fringe per pixel per time difference between the two acquisitions forming the interferogram. For Terrasar-X satellite with a SAR

wavelength of 3.1 cm, and an 11-day orbital cycle, the maximum detectable deformation rate is 0.51 m/y in the line of sight. If the deformation rate exceeds this threshold the signal will be decorrelated. Finally, *Vmax* was computed by dividing this constant by the value of the visibility map for each pixel of the considered landform. Results show that the mode has a big influence on *Vmax* as shown in Fig. 8.

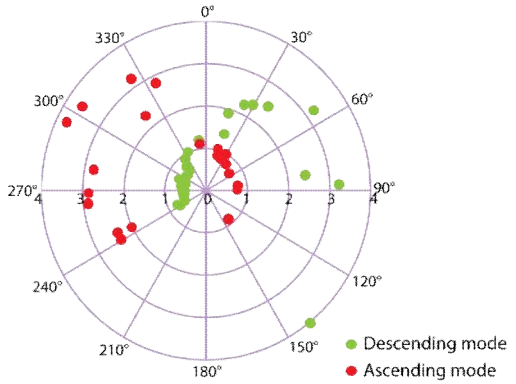

Figure 8: Distribution of the maximal detectable deformation rate (m/y) on the different testing sites located in the Western Swiss Alps in ascending (red) and descending (green) modes according to their aspect

For most of the west-oriented landforms, results show that *Vmax* can reach 1 m/y in descending mode, and 3.5 m/y in ascending mode. The reverse phenomenon appears for east-oriented landforms and *Vmax* usually reaches about 1 m/y in both ascending and descending modes for north-oriented slopes.

The influence of the incidence angle of TSX (full capacity between 20° to 55°) was investigated for each landform to see if it was suitable to survey them with different orbits. Results are shown in fig. 9. For most of the west-oriented landforms, the incidence angle has generally few influences on *Vmax* in ascending mode, which can reaches 7 to 8 m/y for some of these landforms. However, due to steep topography, large layover and distortions could occur on landforms for this mode. In the descending mode, the incidence angle has usually no influence on *Vmax*. The reverse phenomenon appears for east-oriented landforms.

Comparison of *Vmax* and mean velocity landforms known through GPS campaigns show that landforms could be correctly observed in ascending mode. This means that decorrelation does not appear when they are not masked by layover and shadow. However, no extremely rapidly moving rockglacier is observable in descending mode.

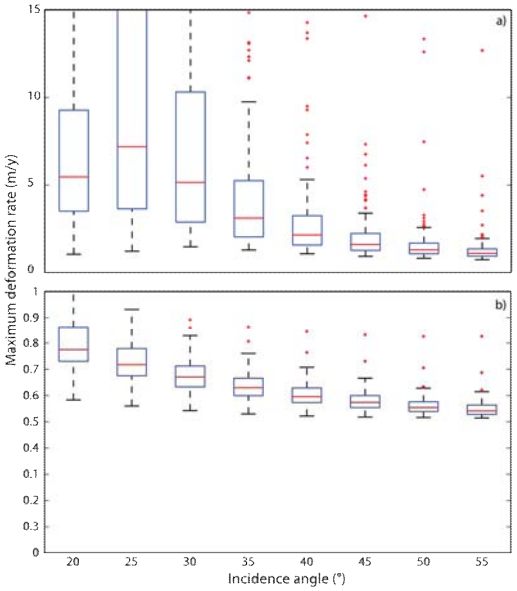

Figure 9 : Typical results of the influence of incidence angle on Vmax a) ascending and b) descending modes (Tsarmine west-oriented rockglacier). The bottom and top of the box, the red line and red crosses show respectively the upper and lower quartiles, the median value and outliers.

5. DISCUSSION

Some comparisons are performed combining InSAR observations and differential local GPS measurements. As a first approximation, the maximal deformation rate is compared to the local velocity of each surveyed GPS point. When the maximal deformation rate is higher to the velocity given by GPS measurement, the point is classified as detectable (in the opposite situation, the point is classified as undetectable).

In most cases, the point classification corresponds to InSAR observation (in term of correlated and decorrelated signal). However, some cases reveal incorrect evaluations of the visibility mainly due to the fact that the maximal deformation rate is not directly related to the velocity (but its derivative). Thus, it is sometimes possible to detect a higher velocity rate than indicated. Past studies using ERS technologies have shown that decorrelation occurs when the velocity rate is up to ə/2 for these kinds of slope instabilities where roughness is an important factor [11]. However it seems to be a higher limit rate for TSX. In Fig. 10, the Tsarmine rockglacier had reached a mean velocity of 1m/y during summer 2010. Its frontal part was moving almost 1.5m/y. As expected with previous results, the area is not decorrelated in ascending mode, and is decorrelated in descending mode. The two red points classified as undetectable on Fig. 10.a are an illustration of the limitation explained before. Comparison between velocity computed by InSAR (using unwrapping process) and GPS measurement are planned to validate more precisely the use of this indicator of visibility.

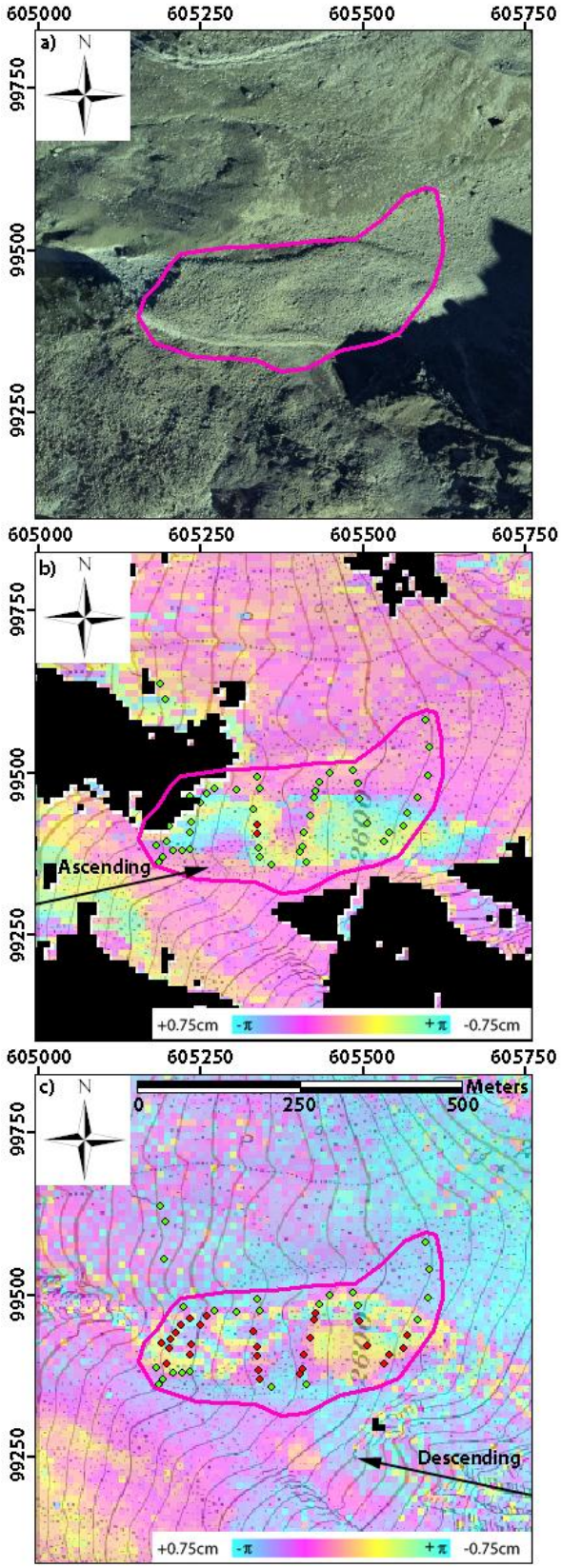

Figure 10 : a) Orthoimage of the Tsarmine rockglacier (2005). Localization of GPS points detectable by InSAR in (b) ascending and (c) descending modes superimposed with InSAR data from 2010 with an 11-day time lag. Green points are detectable with TSX InSAR and red points are undetectable.

6. CONCLUSION

According to the study of this new indicator of visibility, it is possible to monitor some very active rockglaciers (1-3.5m/y) when geometrical distortions do not hide them with the shortest repeat pass of 11 days. Lower velocity rates could be well monitored using longer time lags. At higher rates, decorrelation occurs in most cases and TSX appears to be unsuitable for a precise analysis of these very rapidly moving landforms. Moreover, the high resolution of TSX appears to be suitable for monitoring slope instabilities with narrow width (until 50 meters width). Thus, by combining it with field measurements, needed in most cases to validate and confirm observations at local scale, TSX InSAR has a strong potential for surveying moving landforms of the alpine periglacial belt.

7. ACKNOWLEDGEMENTS

TERRASAR-X data courtesy LAN0411 (c) DLR, DHM25 (c) 2003 Swisstopo, Orthoimages 2005 (c) Swisstopo

8. REFERENCES

1. Delaloye, R., Morand, S. (1997). Du Val Ferret au Grand-Combin (Alpes Valaisannes) : Inventaire des glaciers rocheux et analyse spatiale du pergélisol à lôaide dôun système dôinformation géographique (IDRISI). Travail de diplôme, Inst. Géogr., Univ. Fribourg.

2. Lambiel, C., Reynard, E. (2003). Cartographie de la distribution du pergélisol et datation des glaciers rocheux dans la région du Mont Gelé (Valais). Physische Geographie 41, Geographisches Institut der Universität Zürich, 91-104.

3. Roer, I., Dikau, R., Kääb, A. (2005). Rockglacier acceleration in the Turtmann valley (Swiss Alps): Probable controls. Norsk geog. Tidsskr. 59, 157 ï 163.

4. Roer, I., Haeberli, W., Avian, M., Kaufmann, V., Delaloye, R., Lambiel, C. & A. Kääb (2008). Observations and considerations on destabilizing active rockglaciers in the European Alps. In: Kane, D.L. & K.M.Hinkel (eds): Proceedings of the 9th International Conference on Permafrost, June 29-July 3, 2008, Fairbanks, Alaska 2: 1505-1510.

5. Delaloye R., Lambiel C. & Lugon R. (2005). ESA SLAM project, phase 2, Bas-Valais. Validation of InSAR data in permafrost zone. Unpublished.

6. Delaloye R., Perruchoud E., Lambiel C., Lugon R. (2008), InSAR Haut-Valais: Inventaire des mouvements de terrain par analyse de signaux dôinterférométrie radar satellitaire (période 1993-2000), Rapport final, Mandant: Canton du Valais. Unpublished.

7. Delaloye R., Lambiel C., Lugon R., Raetzo H., Strozzi T. (2006). ERS InSAR for detecting slope movement in a periglacial mountain environment (western Valais Alps, Switzerland). High Mountain Proceedings of the 9th International Symposium on High Mountain Remote Sensing Cartography (HMRSC-IX), Graz, Austria, 14-15 Sept. 2006.

8. Delaloye R., Strozzi T., Lambiel C., Perruchoud E., Raetzo H. (2008). Landslide-like development of rockglaciers detected with ERS1-2 SAR interferometry. Proc. of FRINGE 2007 Workshop, Frascati, Italy, 26 ï 30 November 2007 (ESA SP-649, February 2008).

9. Delaloye R., Strozzi T., Lambiel C., Barboux C., Mari S., Stocker A., Techel F., Raetzo H. (2010). The contribution of InSAR Data to the early detection of potentially hazardous active rock glaciers in mountain areas. Proceedings ESA Living Planet Symposium 2010, Bergen, Norway (ESA SP-686).

10. Lambiel C., Delaloye R., Strozzi T., Lugon R., Raetzo H. (2008). ERS InSAR for Assessing Rock Glacier Activity. Proceedings of the 9th International Conference on Permafrost, Fairbanks, Alaska, USA, June 29 - July 3, 2008.

11. Delaloye R., Lambiel C., Lugon R., Raetzo H., Strozzi T. (2007). Typical ERS InSAR signature of slope movements in a periglacial mountain environment (Swiss Alps). Proceedings of the Envisat Symposium, Montreux, Switzerland, 23-27 April 2007.

12. Strozzi T., A. Kääb and R. Frauenfelder (2004). Detecting and quantifying mountain permafrost creep from in situ inventory, space-borne radar interferometry and airborne digital photogrammetry. Int. J. Remote Sensing, Vol. 25, No. 15, 2919-2931.

13. Kropatsch W.G. and Strobl D. (1990). The generation of SAR Layover and Shadow maps from digital elevation model. IEEE Transactions on Geoscience and Remote Sensing, Vol. 28 No 1, January 1990.

14. Massonet D., Feigl K.L. (1998). Radar interferometry and its application to changes in the earthôs surface. Reviews of Geophysics, 36, 4 / November 1998, 441ï 500.